Colloids and Surfaces A: Physicochem. Eng. Aspects 494 (2016) 30–38

Contents lists available at ScienceDirect

Colloids and Surfaces A: Physicochemical and Engineering Aspects

journal homepage: www.elsevier.com/locate/colsurfa

Ion effects in the adsorption of carboxylate on oxide surfaces, studied with quartz crystal microbalance

Lei Wang*, Igor Siretanu, Michel H.G. Duits, Martien A. Cohen Stuart, Frieder Mugele

Physics of Complex Fluids Group, MESA+ Institute, University of Twente, P.O. Box 217, 7500 AE Enschede, the Netherlands

HIGHLIGHTS

- Carboxylate adsorption on mineral surfaces is studied with Quartz Crystal Microbalance.
- On silica, Ca^{2+} can promote carboxylate adsorption via ion-bridges.
- On alumina, carboxylates adsorb mainly via ligand exchange, even in presence of Ca^{2+}.
- On gibbsite, carboxylates and Cl^- adsorb competitively via pre-adsorbed Ca^{2+}.

GRAPHICAL ABSTRACT

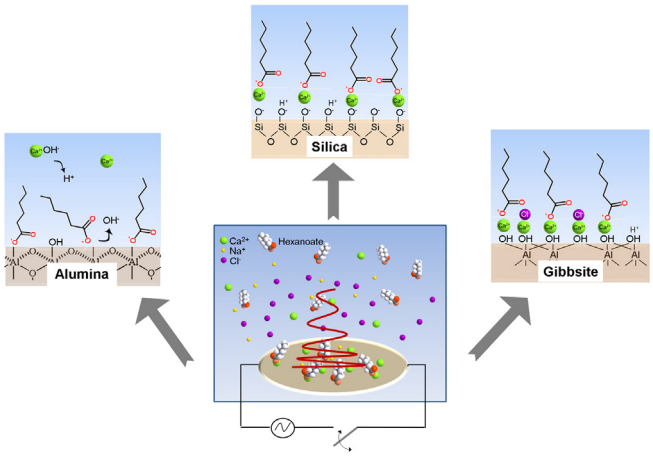

ARTICLE INFO

Article history:
Received 30 November 2015
Received in revised form 12 January 2016
Accepted 13 January 2016
Available online 16 January 2016

Keywords:
Adsorption
Oxide surfaces
QCM-D
Ligand exchange
Cation bridging

ABSTRACT

We chose water-soluble sodium hexanoate as a model organic molecule to study the role of salt ions (Ca^{2+}, Na^+, Cl^-) in the adsorption of carboxylates to mineral surfaces (silica, alumina, gibbsite) of variable surface charge and chemistry. Quartz crystal microbalance (QCM-D) measurements reveal a qualitatively different dependence of the adsorption behavior on the electrolyte composition for the different surfaces at near neutral pH. Overall, hexanoate adsorption is more pronounced on the positively charged alumina surfaces than on negatively charged silica surfaces. On silica, however, Ca^{2+} ions strongly enhance the adsorption of hexanoate, suggesting that the divalent cations act as bridges between carboxylate and deprotonated silanol surface groups. On alumina, hexanoate adsorption is found to depend only weakly on the salt composition, suggesting a direct interaction of the carboxylate group with the surface, consistent with a ligand-exchange mechanism. The adsorption behavior on partially gibbsite-covered silica surfaces is particularly rich and displays a strong non-monotonic dependence on the $CaCl_2$ concentration. Comparison to earlier work and control experiments suggest an important role of Cl^- anions, which compete with the carboxylate group for adsorption sites.

1. Introduction

Adsorption of organic molecules and other species at mineral (clay) water interfaces has been studied for a long time but still

* Corresponding author.
E-mail address: l.wang@utwente.nl (L. Wang).

http://dx.doi.org/10.1016/j.colsurfa.2016.01.019
0927-7757/

attracts great interest of researchers. This is because the adsorption phenomena can have a multitude of effects: they can alter the wettability of macroscopic substrates [1], tune the rheology of particle suspensions [2], modify the sorptive properties [3], etc. As a result, this phenomenon is critical to many industrial applications such as water treatment [4], nanocomposites fabrication [5] and oil recovery [6,7].

Clay also known as phyllosilicate, mainly consists of aluminosilicate layers, containing silicon dioxide tetrahedral sheets and aluminum oxyhydroxyl octahedral sheets. Therefore in many fundamental studies silica, alumina or gibbsite are used as models of clay minerals. In particular, studies on interactions between organic molecules like carboxylates and the above mineral surfaces have been conducted [8–12], because carboxylates are commonly found in nature as well as in industrial processes. Effects of pH and ionic strength on the adsorption process have been well covered by several works [8,12–15]. However, only few studies were so far aimed at comparing the adsorption behaviors of carboxylates on different substrates and at different aqueous ion compositions (including salt mixtures). An exception is the recent work of Juhl, who reported that the bonding strength between a carboxylate and an alumina surface changes with the solution salinity, and that divalent ions can replace adsorbed monovalent ions on oxide surfaces [16]. Understanding the adsorption mechanism of carboxylates at the different clay surfaces, including the competition between ions during this process, would help to understand many industrial processes.

A good example is given by the water flooding process, which is routinely practiced in oil recovery to release (more) hydrocarbons from the subsurface. Traditionally, (highly saline) sea water is injected into the rock reservoir to repel the mobilized oil from the rock surface. However, it was recently found that the recovery can be enhanced by flooding with low salinity solutions [17,18]. This low salinity effect has been attributed to an alteration of the wettability: the rock becomes more water-wet when organic material is desorbed from the clay surface. However the underlying microscopic mechanisms behind the ad/desorption of organic molecules and other species at clay-mineral surfaces are still not clarified. In previous works, some progress was made along this line. Langmuir–Blodgett films were studied to demonstrate the role of divalent cations as bridging ions between silica substrates and stearic acid molecules [19]. Additionally, atomic resolution AFM was used to examine specific ion adsorption on gibbsite surfaces [20].

In this paper, we investigate the adsorption of a water soluble, short-chain carboxylate (hexanoate) on various oxide surfaces (silica, alumina and gibbsite). The aim is to understand the role of cations in particular from mixed electrolytes on the adsorption of carboxylate, as well as the adsorption mechanism of carboxylate on these oxides. The pH value was chosen to be around 7, which is close to the natural conditions. In this regime, the dissociation of the carboxylic acid and the surface charges of the oxides (silica, alumina and gibbsite) surfaces are all sensitive to the pH. Besides different concentrations of hexanoate, also various compositions of NaCl and $CaCl_2$ solutions were explored.

The principal technique we have used is the measurement of adsorbed mass using a Quartz Crystal Microbalance capable of quantifying also dissipation (QCM-D). Careful application of this sensitive method allowed us (for the first time) to perform semi-quantitative measurements of the adsorption isotherm for these very small molecules. To support our data analysis, also Atomic Force Microscopy (AFM) experiments were performed; these measurements provided information about the state of charge of the bare substrates. Based on the combined data, adsorption mechanisms on different solid surfaces are proposed.

2. Experimental

2.1. Materials

Sodium hexanoate (C6), Hexanoic acid, $CaCl_2{\cdot}2H_2O$, and NaCl were obtained from Sigma–Aldrich and used without further purification. Deionized water with a resistivity of 18.2 MΩ cm (Synergy-UV, Millipore) was used throughout this study.

Silica-coated and alumina-coated quartz crystal sensors were purchased from Q-sense (Gothenburg, Sweden). A suspension of gibbsite nanoparticles was kindly provided by the group of Prof. A.P. Philipse (University of Utrecht, the Netherlands). Synthesis and characterization of the material were described by Wierenga et al [21]. The gibbsite-coated sensor was prepared by depositing gibbsite particles from a suspension on the silica coated quartz crystal, following the procedures described by Siretanu et al. [20].

2.2. AFM imaging and force spectroscopy measurements

Topographical features of the QCM sensor surfaces were studied by using a Multimode8 Atomic Force Microscope with a Nanoscope V controller (Bruker Nano). A Dimension Icon AFM (Bruker) equipped with a Nanoscope V controller was used to study the surface charge of the sensors. All samples were analyzed in amplitude modulation mode. Silicon tips from MikroMasch, NSC36 (f_0 = 52 kHz, c_z = 3.6 N/m, Q = 4.8, tip radius ~19 nm) and Bruker FASTSCAN-B cantilevers (f_0 = 170 kHz, c_z = 3 N/m, Q = 10, tip radius ~3 nm) were used. Before the measurement, both the tip and cantilever were rinsed with an ethanol/isopropanol (≈1:1) mixture and treated further with air plasma (Harrick Plasma) for 15 min. Image analysis was carried out with Nanoscope Analysis version 120 software (Bruker). Roughness data were extracted from three separate images obtained at different regions on each sample. The surface coverage of gibbsite sensor was 55% ± 10%. The surface charge of the substrates in electrolyte solution was determined from analysis of AFM interaction stiffness (force gradient) versus distance curves in the framework of DLVO theory, complemented by a charge regulation boundary condition. The AFM equipment, the operations, and details about force inversion and charge extraction have been described elsewhere [22,23].

2.3. Adsorption measurements by QCM

Adsorption experiments were performed as a function of the Na-hexanoate (C6) and salt concentrations. On each sensor, three concentration series were examined. In each of the series, the concentration of C6 was varied from 0 to 10 mM. Since this is far below the solubility (70 mM) [24,25], no precipitation should occur. The total Na^+ concentration (from C6 and NaCl) was always maintained at 10 mM, while the concentration of $CaCl_2$ was controlled at 0, 10 and 20 mM. In short, these series are denoted as: 1) C6-Na; 2) C6-Na-10Ca and 3) C6-Na-20Ca. The pH of the samples varies from 6 to 7 with the concentration of C6. Because hexanoic acid is a weak acid (pK_a = 4.85), the carboxylate groups will occur partly in protonated and partly in deprotonated form. According to Lee [26], at pH 7 the Critical Micelle Concentration (CMC) of Na-carboxylate is approximately 1 M, and that of Ca-dicarboxylate is higher than 0.03 M [27,28]. Our solutions are always more diluted than this, so that we can safely exclude the presence of micelles.

Adsorption studies are conducted with the QCM-D (E4) instrument from Q-sense (Gothenburg, Sweden). A standard AT-cut quartz crystal sensor with a diameter of 14 mm has a 100 nm thick gold layer as electrode. In our case silica-, alumina- and gibbsite-coated sensors were used. The QCM-D liquid chamber is mounted on a Peltier element, which controls the temperature accurately (at 22 ± 0.1 °C) to avoid signal drifts. The fundamental oscillation

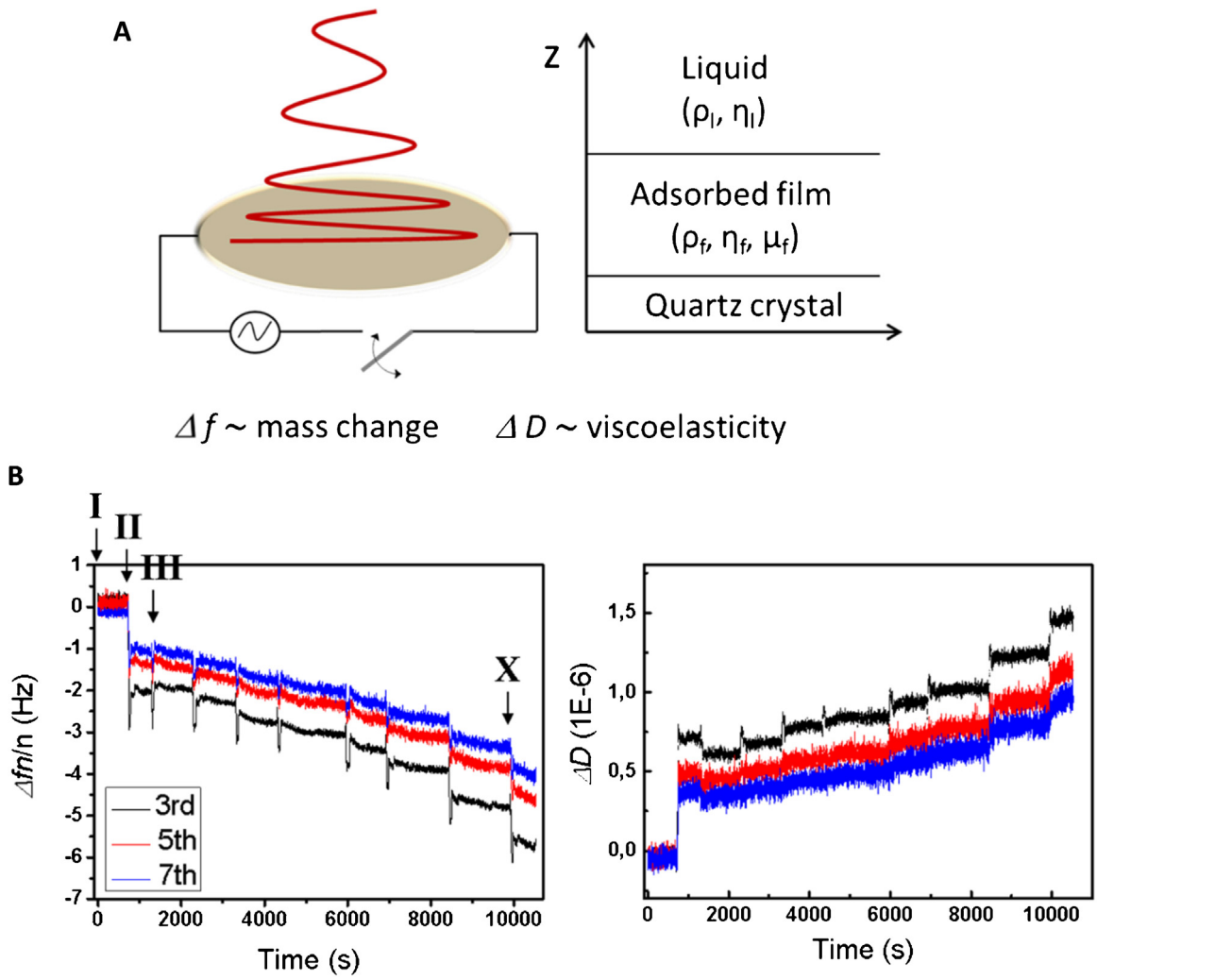

Fig. 1. (A) Schematic illustration of quartz crystal microbalance principle; (B) frequency and dissipation shift recorded with different solutions injected sequentially: water (I), aqueous salt solution (II); (III) to (X) are hexanoate (C6) solutions with the same salt concentration as in (II), while the C6 concentration varies from 0.1 to 10 mM.

frequency of the crystal is 5 MHz. Changes in frequency and dissipation are recorded simultaneously at 5, 15, 25, 35... MHz. All measurements are started with DI water, followed by the background salt solution (containing Na^+ and/or Ca^{2+}), and then the series of C6 solutions from low to high concentrations, as demonstrated in Fig. 1. The solution was sucked into the chamber with a peristaltic pump. The pump was stopped after the chamber was filled with fresh solution. Frequency and dissipation signals were recorded continuously. At the moment that a plateau was reached (for both), the next sample solution was sucked into the chamber. Since the molecules studied in this work are very small, contamination of the small measurement signals had to be avoided as much as possible. Drift was minimized by preparing the experimental setup and the samples overnight before each measurement.

2.3.1. Principle of QCM-D and data analysis

Since QCM plays a prominent role in this study, a brief background is given. The Quartz Crystal Microbalance (QCM) technique is well-known for characterizing adsorbed mass at solid surfaces. It is based on the piezoelectric effect. When an alternating potential is applied to the electrodes, shear stresses is generated in the piezoelectric material, causing the crystal to oscillate at a resonant frequency. Changes in the mass (Δm) bound to the crystal surfaces cause a shift of the resonance frequency (Δf). In the absence of significant damping by the ambient environment, the Sauerbrey relation can be used [29]:

$$\Delta f = \frac{-f_o}{t_q \rho_q} \times \Delta m = \frac{-n \times \Delta m}{C} \quad (1)$$

where ρ_q is the mass density of the quartz, f_o is the fundamental frequency, and t_q is the thickness of the quartz crystal. C is the mass sensitivity constant ($C = 17.7\ \mathrm{ng\,cm^{-2}\,Hz^{-1}}$ at 5 MHz), and n indicates the overtone number ($n = 1, 3, \ldots$). The conditions for Eq. (1) to hold are that: (i) the adsorbed mass is evenly distributed over the sensor; (ii) the adsorbed mass is much smaller than that of the crystal; (iii) the adsorbed film should couple perfectly with the shear oscillation of the sensor. The latter is not always the case, especially if the adsorbed film is viscous and does not follow the mechanical oscillation of the sensor. In this case, the frequency shift also depends on the viscous and elastic nature of the adsorbed film. In QCM-D, the dissipation of a sensor's energy (D), due to the adsorbed viscoelastic layer is also recorded. The dissipation (D) is given by:

$$D = \frac{1}{Q} = \frac{E_d}{2\pi \times E_s} \quad (2)$$

where Q is the quality factor, E_d is the energy dissipated in one period of oscillation, and E_s is the energy stored in the oscillation system. The measurement of D allows for a more accurate estima-

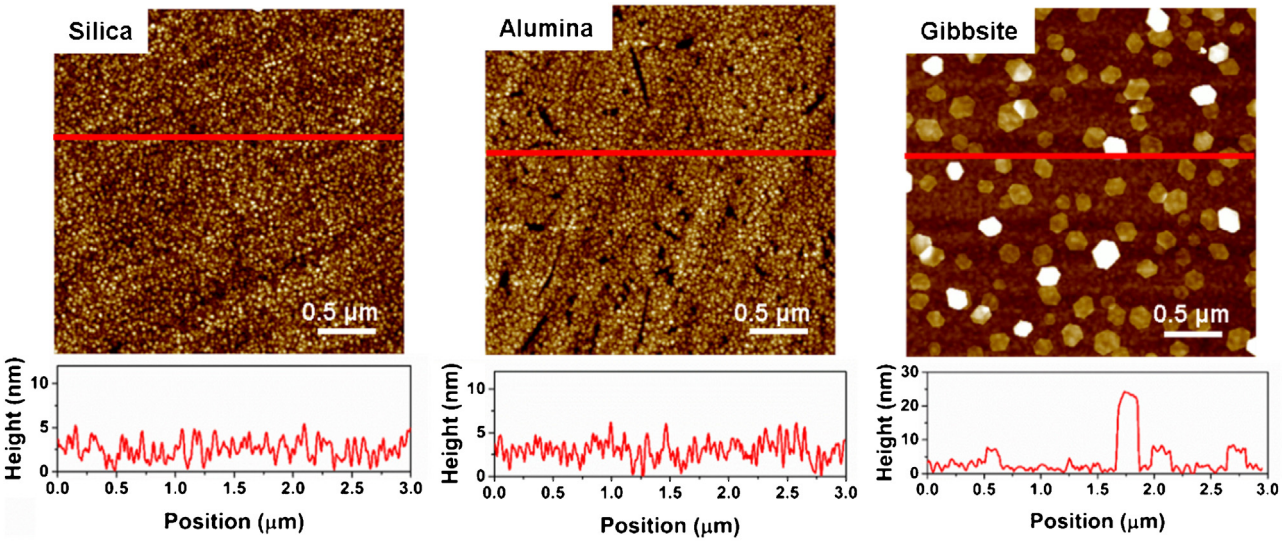

Fig. 2. Topographical features of silica, alumina, gibbsite-silica sensors in water and their corresponding height profile.

tion of the adsorbed mass in a non-rigid film by introducing the viscosity and shear modulus in the modeling.

In the Sauerbrey equation, the adsorbed mass is proportional to the normalized frequency shift, which is independent of the overtone number. However in our case, shown in Fig. 1 for a typical dataset, the frequency shift presents an overtone dependent behavior. This suggests that the adsorbed layer might not be perfectly rigid. Therefore, we use, instead, the Voigt-based model [30,31] for the data analysis, which is implemented in the 'Q-tool' software from Q-sense. In this model, the adsorbate is represented a homogeneous layer (film, as shown in Fig. 1A) on the sensor surface with density, viscosity and shear modulus: (ρ_f, η_f, μ_f); the properties of bulk solution (liquid, as displayed in Fig. 1A) are represented by (ρ_l, η_l) for which we used 1002 kg/m^3 and 0.001 kg/m s, respectively. The expected mass density of a close packed organic monolayer is 958 kg/m^3, assuming upright hexanoate molecules with a head group of 20 Å^2 [19] and molecular length of 1 nm [32]. Hence in the modeling, only η_f, μ_f and the adsorbed mass are used as fit parameters. Data from at least three overtones with good signal to noise ratio are therefore needed. The first overtone is not used as it senses mostly the solution and is affected by the clamping [33]. In this work, data from 3rd, 5th, 7th, 9th, 11th overtones are used to find the adsorbed mass because they display stable responses.

Since QCM is an acoustic technique, it cannot discriminate between different chemical species. Hence the number density of individual adsorbed ions and molecules cannot be extracted from the total adsorbed mass. Moreover, water may couple as additional mass due to hydration, or entrapment in the cavities in the adsorbed layer as observed in other work [30]. Therefore our results do not represent, in a strict sense, adsorption isotherms, although they follow very similar trends, and we will refer to them as 'adsorption curves'. Consequently, we refrain from converting the data into chemical units (mol cm^{-2}) but present them in weight units (ng cm^{-2}).

3. Results and discussion

3.1. Characterization of silica, alumina and gibbsite-silica sensors

Electrostatic interactions are generally recognized as an important driving force for the adsorption of organic or inorganic ions at solid–liquid interfaces. Since the oxide surfaces used in this work are prone to get charged in contact with aqueous solutions, understanding of ion adsorption should be facilitated by characterization of the electrical state of the substrates.

Fig. 2 displays typical height images of the three types of QCM sensors used in this study. Generally, silica and alumina coated sensors present rather smooth surfaces: the height variations have a root-mean square amplitude of 1.2 ± 0.028 nm and 1.6 ± 0.021 nm respectively, and also the gradients in height are very small (note that the line scans in Fig. 2 are strongly compressed in the horizontal direction). This is also confirmed by the height maps, from which we infer a "true" surface area (i.e. by taking into account the areas of "hills" and "valleys" of the surface contour) that is 9.08 and 9.11 μm^2 within 9 μm^2 imaging area, for silica and alumina respectively. The gibbsite-silica sensor demonstrates the typical hexagonal gibbsite particles, with a typical lateral dimension of 100 nm, and heights from 5 to 20 nm, due to the aggregation (stacking) of gibbsite platelets. From the height images, we can estimate the effective surface area of gibbsite-silica surfaces, which is 9.02 μm^2 corresponding to 9 μm^2 imaging area. QCM experiments on gibbsite surfaces were performed with the same sensor, which has a stable coverage of gibbsite (≈55%) through all the measurements.

The effective surface charges of the three sensor surfaces were measured at the same electrolyte compositions as used in the adsorption studies. Fig. 3 presents the force gradient (interaction stiffness) as a function of tip sample distance. On silica surfaces (black symbols in Fig. 3A and B), the tip experiences a repulsion, which increases monotonically as the tip approaches the surface. This suggests a system of two negatively charged surfaces. On alumina (magenta symbols in Fig. 3A) and gibbsite (orange symbols in Fig. 3 B), the silica tip experiences attraction, indicating an oppositely charged substrate. The observed dependence on the concentration and composition of the salt shows the combined effect of changes in the ion adsorption and in the diffuse double layer.

To obtain more quantitative information, the surface charges were extracted from the interaction stiffness curve using extended DLVO theory, where Charge Regulation (CR) effects, i.e. variations of the surface charge due to confinement-induced ion adsorption, (de) protonation of surface groups, etc., are taken into consideration. For more details, see Ref. [23]. The minimum tip-sample distance used for fitting was set to 1 nm, to minimize the influences of short-range forces such as hydration forces, which are not included in the model. The upper boundary was set to 10 nm, because the

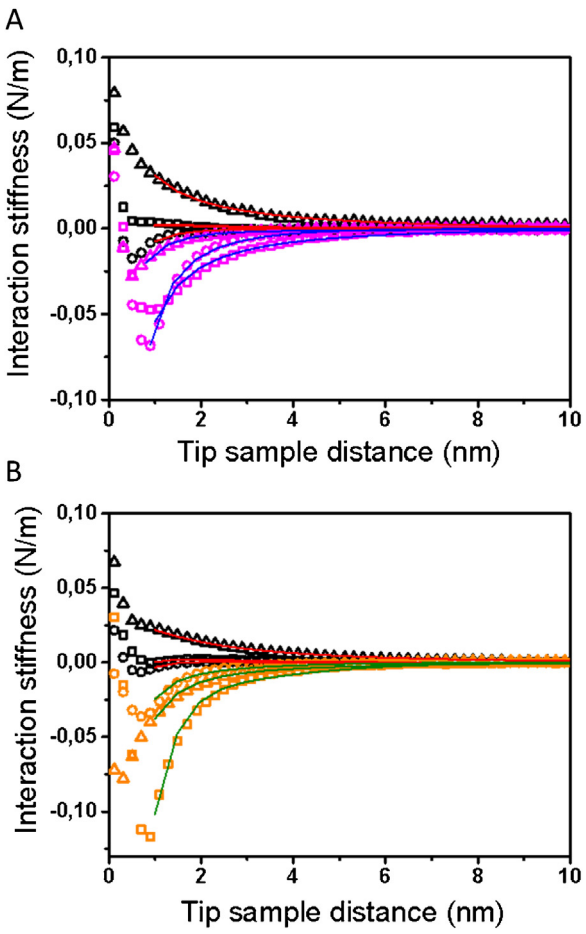

Fig. 3. Interaction stiffness versus distance measured between a silicon oxide tip and sensor surfaces: silica (black symbols), alumina (magenta symbols in A) and gibbsite (orange symbols in B). Symbols are experimental data: 10 mM NaCl (triangle), 10 mM NaCl −10 mM $CaCl_2$ (square), and 10 mM NaCl −20 mM $CaCl_2$ (circle). Solid lines are the theoretical calculation. The surface charge values from this fitting are presented in Table 1. (For interpretation of the references to color in this figure legend, the reader is referred to the web version of this article.)

Table 1
Surface charge densities of the three sensors, in contact with different solutions.

	Surface charge (e/nm^2)		
	10 mM NaCl	10 mM NaCl–10 mM $CaCl_2$	10 mM NaCl–20 mM $CaCl_2$
Silica	−0.060	−0.019	−0.020
	−0.062	−0.020	−0.018
Alumina	0.013	0.015	0.023
Gibbsite	0.023	0.125	0.025

Note: Surface charge on silica was extracted from two measurements, see Fig. 3A and B.

interactions are negligible beyond this distance. Fig. 3 shows that there is a good agreement between the theoretical curves and the experimental results. The extracted surface charge densities are summarized in Table 1.

On the silica surface in 10 mM NaCl solution, the charge density is found to be −0.06 e/nm^2, while it becomes −0.02 e/nm^2 upon addition of 10 or 20 mM $CaCl_2$. This behavior is attributed to an adsorption of the Ca^{2+} ions onto the silica, which probably also involves deprotonation, i.e. replacement of Si—OH by Si—OCa^+.

Both alumina and gibbsite display positively charged surfaces for the electrolytes investigated. On alumina, the surface charge increases upon the addition of $CaCl_2$. This could be interpreted as a result of the buffering effects of Ca^{2+} ions, which are capable of

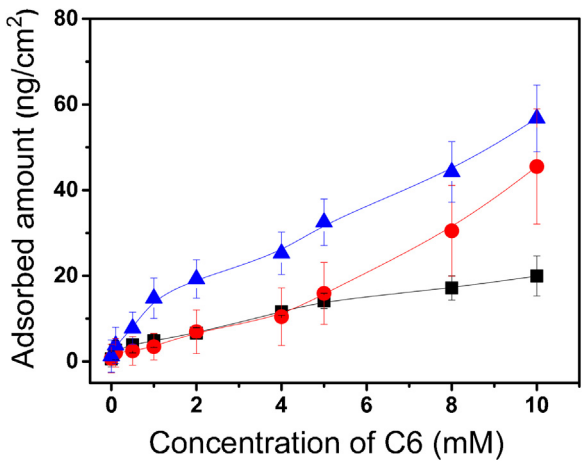

Fig. 4. Sodium hexanoate (C6) adsorption on silica surfaces in presence of salts: (i) 10 mM Na ions (black squares); (ii) 10 mM Na ions +10 mM $CaCl_2$ (red circles); (iii) 10 mM Na ions +20 mM $CaCl_2$ (blue triangles). Lines are drawn for guiding the eye. (For interpretation of the references to color in this figure legend, the reader is referred to the web version of this article.)

forming $Ca(OH)^+$ [34] and thereby lowering the pH contributing to the increase in surface charge. Moreover, Ca^{2+} might replace the protons at alumina surfaces which also enhances the surface charge.

Remarkably, the surface charge density on gibbsite, shows a maximum at the intermediate (i.e. 10 mM) $CaCl_2$ concentration. This complies with a previous study [20] where it was interpreted in terms of specific ion adsorption. The excess positive charge as compared to monovalent cations, can be explained with an adsorption of Ca^{2+} ions on the gibbsite surface. The decrease in net surface charge at higher $CaCl_2$ concentrations, might be explained by adsorption of Cl^- onto the already adsorbed Ca^{2+}.

3.2. Adsorption of hexanoate

3.2.1. Silica surfaces

Fig. 4 displays the adsorption curves of hexanoate on silica. Without $CaCl_2$, the maximum adsorption density (Γ) (at 10 mM C6) is only around 20 ng cm^{-2}, much less than a densely packed monolayer ~100 ng cm^{-2} (with the molecular weight of 115 g/mol, and the size of carboxylate head group around 20 Å^2 [19]). With 10 mM $CaCl_2$, and below 5 mM C6, the [C6] dependent adsorption overlaps with the Ca- free case. Above 5 mM C6, the adsorption increases more steeply. With 20 mM $CaCl_2$, the adsorption shows a steep initial increase. The difference between the cases of 10 and 20 mM $CaCl_2$ then remains more or less constant as [C6] is increased. The overall picture that emerges, is that (above certain thresholds for [$CaCl_2$] and [C6]), adding more $CaCl_2$ results in a larger adsorbed mass.

To explain this trend, we consider the charge on the silica surface (in absence of C6). At pH ~7 the silica surface is negative, as also corroborated by the AFM measurements (Table 1). Most hexanoate molecules are in the form of —COO^- at pH ~7 because hexanoic acid is a weak organic acid with a pK_a = 4.85 [35]; this makes adsorption of C6 unfavorable from an electrostatic point of view. Indeed, only small amounts of hexanoate adsorb from solutions of only C6-Na. The fact that a similar behavior was found with hexanoic acid at similar pH on silica surfaces (results not shown), suggests that Na^+ ions cannot provide strong assistance to the adsorption of C6 on silica. The observation that some adsorption still occurs, and that the amount grows with [C6], might be attributed to weak Van der Waals-London dispersion forces between the alkyl tail and the silica. Weak hydrophobic interactions between neighboring adsor-

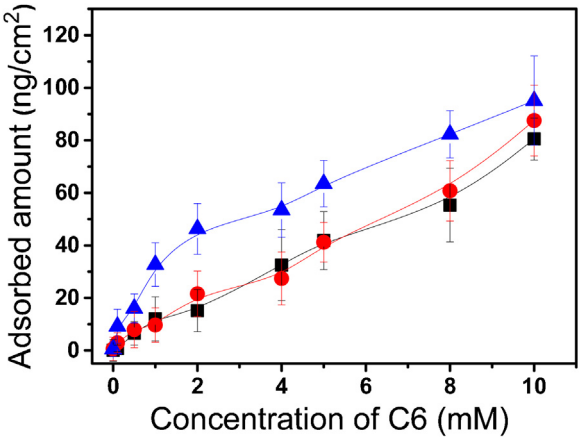

Fig. 5. Sodium hexanoate (C6) adsorption on alumina surfaces: (i) with 10 mM Na ions (black square); (ii) with 10 mM Na ions +10 mM $CaCl_2$ (red circle); (iii) with 10 mM Na ions +20 mM $CaCl_2$ (blue triangle). Lines are drawn for guiding the eye. (For interpretation of the references to color in this figure legend, the reader is referred to the web version of this article.)

bates might offer additional assistance to the adsorption. However, this effect can only be small, and in that case expected S-shaped isotherm is not observed.

In the presence of Ca^{2+}, significantly larger amounts are adsorbed, and the more so for higher $CaCl_2$ concentration. Similar effects of divalent cations have also been reported in another study [36]. Another work has found that Langmuir–Blodgett films of stearic acid on silica display higher stability when prepared in presence of Ca^{2+}, as compared to Na^+ [19]. These findings are consistent with an adsorption that is strongly facilitated by the (electrostatic) effects of divalent cations. Apparently, the latter are very effective in establishing cation bridges between a negative surface and the negative hexanoate ion [37].

The observation that the maximum adsorbed amounts are relatively low, and that adding more Ca^{2+} to a system where $[Ca^{2+}]/[C6]$ was already » 1 leads to more adsorption, indicates that the adsorption is weak, and governed by chemical equilibrium. In this picture, the Ca^{2+} ions in solution form partially dissociated, cationic complexes with carboxylic acid:

$$Ca^{2+} + {}^{-}OOC\text{-}R \leftrightarrow R\text{-}COOCa^{+} \quad (3)$$

At the silica surface, most likely Ca monohexanoate (with the Ca facing the mineral surface) is the dominant species. The enhancement of the adsorption by both Ca^{2+} and hexanoate is also consistent with the increase in the initial slope for higher $[Ca^{2+}]$ as seen in Fig. 4.

3.2.2. Alumina surfaces

On alumina surfaces, the adsorption of C6 is much stronger than on silica. As shown in Fig. 5, the adsorbed mass per unit area (Γ) approaches 80 ng cm^{-2} at the highest [C6], even in the absence of Ca^{2+}, where it only reached ~20 ng cm^{-2} on silica (Fig. 4). Adding 10 mM $CaCl_2$ to the system has remarkably little effect on the maximum adsorbed amount at 10 mM C6; also this is different from the case of silica, where adding $CaCl_2$ gives rise to a stronger relative increase in Γ. Another remarkable observation is that at the intermediate $CaCl_2$ concentration of 10 mM, the adsorption isotherm does not appear to be significantly different from that of the pure C6-Na.

Also in this case, charge interactions are expected to play an important role. In contrast to the silica surface, the alumina is slightly positively charged at pH ~7. Since most carboxylate molecules are deprotonated and thus negatively charged at that pH, electrostatic attractions should be present. It is plausible that this causes the larger adsorbed amounts. However, the complex dependence on the $CaCl_2$ concentration (no detectable difference on adding 10 mM, but a significant increase in Γ at 20 mM) suggests that electrostatics alone is insufficient to explain our observations.

Other indications for this can be found in literature. For electrostatically driven adsorption, the maximum amounts should be found at a pH somewhere between the point of zero charge of alumina and the pK_a of the carboxylic acid: the solid surface is then positively charged while most carboxylate groups are deprotonated. However, several researchers [9–12,26] have reported maximum adsorption at pH values close to the pK_a of carboxylate. Kummert [9] found that the tendency of carboxylic acid to form complexes on alumina surfaces is similar to that of organic ligands to form complexes with Al^{3+} in solution. Vermöhlen [38] found that the carboxylate oxygen can bind to the alumina surface, resulting in a ligand-exchange complex. Lee et al. [26] studied carboxylate adsorption on alumina systematically as a function of pH, and also concluded that ligand-exchange is the dominant mechanism of adsorption. Here, the carboxylate group exchanges with the hydroxyl group:

$$> Al - OH + {}^{-}OOC - R \leftrightarrow > Al - OOC - R + OH^{-} \quad (4)$$

At low pH, most carboxylate ions are protonated. Due to the limited number of $^{-}$OOC-R groups in solution, little adsorption can then occur. At very high pH, hydroxide ions compete for the adsorption sites on alumina, also resulting in little adsorption. At a certain intermediate pH within the above large range (including the pK_a value) the maximum adsorption occurs.

It is thus plausible that pH is the dominant factor in the ligand-exchange process. In the solutions studied in this work, both Ca^{2+} and hexanoate can act as a pH buffer. For Ca^{2+} this is due to its ability to form $CaOH^+$ complexes in aqueous solution [34]. Experimental evidence for this was found in a decrease in pH from 5.8 to 5.3, upon addition of 20 mM $CaCl_2$ to a 10 mM NaCl solution. Hexanoate forms a classical buffer system, in which the pH is governed by the ratio $[-COO^-]/[-COOH]$. This ratio varies with the initial concentration of sodium hexanoate. The pH of the solutions thus varies slightly from 6 to 7 on increasing the C6 concentration.

The similar pH values of the C6-Na and C6-Na-10Ca solutions, could thus explain why only few differences are observed between their adsorption curves. In the C6-Na-20Ca system much more free Ca^{2+} ions are present, especially at low C6 concentration. These can then play a stronger role as a buffer, and shift the pH toward the pK_a value. This might explain the steep increase in adsorption at low [C6]. At the higher C6 concentrations, the pH values are more similar for all systems, as they become more dominated by the ratio of $[-COO^-]/[-COOH]$.

While it is clear that the solution pH plays an important role in the adsorption on alumina, it cannot be ruled out that cation adsorption (in spite of the unfavorable charge interaction) can contribute to the phenomenon as well (e.g. via ion bridging). XPS measurements on alumina that was exposed to a mixed solution of NaCl and $CaCl_2$ revealed that only Ca^{2+} ions had adsorbed [16]. While this points at an (ion-) specific role for (at least) the calcium, our experiments do not provide an unambiguous connection with the adsorption of C6. The very similar charge densities (Table 1) and adsorption curves for the solutions with 10 mM NaCl and with 10 mM NaCl +10 mM $CaCl_2$ does not suggest a strong sensitivity to Ca^{2+} as a specific species.

3.2.3. Gibbsite-silica surfaces

The adsorption of hexanoate on the mixed gibbsite-silica sensor displays a remarkable non-monotonic dependence on the $CaCl_2$ concentration, see Fig. 6. Maximum adsorption occurs for the system with 10 mM $CaCl_2$. Here the adsorption increases steeply at low C6 concentration, and approaches a plateau for higher [C6],

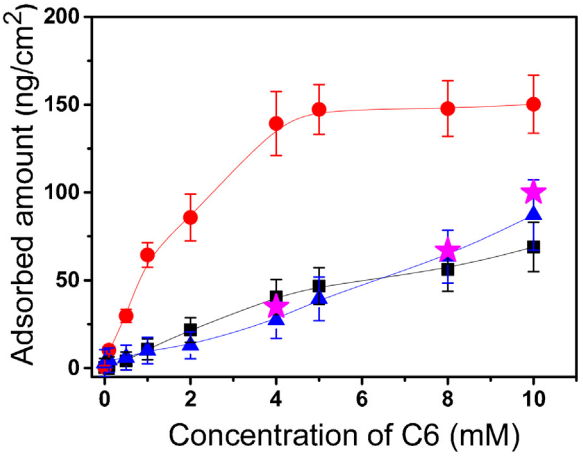

Fig. 6. Sodium hexanoate (C6) adsorption on 55% Gibbsite covered silica surfaces: (i) with 10 mM Na ions (black square); (ii) with 10 mM Na ions and 10 mM $CaCl_2$ (red circle); (iii) with 10 mM Na ions and 20 mM $CaCl_2$ (blue triangle); (iv) is (ii) with additional 10 mM NaCl (magenta stars). (The lines are drawn for guiding the eye.). (For interpretation of the references to color in this figure legend, the reader is referred to the web version of this article.)

indicating a saturated adsorption. Remarkably few differences are found between the adsorption curves for the systems without $CaCl_2$ and with 20 mM $CaCl_2$, both of which are very different from the 10 mM $CaCl_2$ case. In these cases the adsorbed amount increases steadily with C6 concentration, and no plateau is observed up to 10 mM C6.

The sensor has a gibbsite surface coverage of ~55%. Using this number together with the adsorption masses per unit area (Γ) on the pure silica from Fig. 4, we can calculate the adsorption densities on the gibbsite, which are 109, 235, and 111 ng cm^{-2} for the C6-Na, C6-Na-10Ca and C6-Na-20Ca systems, respectively. These amounts are much higher than those on silica or alumina, indicating a very different adsorption behavior on gibbsite.

Gibbsite is one of the most common aluminum hydroxide phases. One key aspect of gibbsite is that it displays Lewis acid-base properties [39]: it can interact with both cations and anions, depending on chemical conditions. The adsorption or bonding mechanism of dicarboxylate on gibbsite has been studied before [14]. Similar to the adsorption on alumina, this is also a ligand-exchange process. However, as we can see from Figs. 5 and 6, the adsorption curves look (qualitatively and quantitatively) rather different from those on alumina.

We ascribe these differences to the fact that Gibbsite is a crystalline solid, with a clear lattice structure. Unlike the case of alumina, divalent ions (Ca^{2+}) can now strongly bind to well-defined adsorption sites forming periodical double row structures, see Fig. 7, while Na^+ or Cl^- ions attach only weakly to the crystal surfaces [20]. In the presence of Ca^{2+} ions, hexanoate molecules can attach to the gibbsite surfaces via these pre-adsorbed divalent ions (Fig. 7), leading to a significant increase in the adsorbed mass for 10 mM $CaCl_2$. However, increasing the $CaCl_2$ concentration by 10 mM leads to a decrease in Γ, making it roughly similar to the case without $CaCl_2$. This is probably due to a high concentration of Cl^- ions, which compete for the adsorption sites with hexanoate.

To support the latter hypothesis, another adsorption experiment was conducted with the same gibbsite coated sensor. In this measurement, an additional 10 mM NaCl was added to the C6-Na-10Ca system (see the stars in Fig. 6). The adsorbed amount indeed decreases, close to the value of C6-Na-20Ca. As Na ions cannot bind to gibbsite surfaces [20]. their effects on carboxylate adsorption can be neglected. This furtherly confirms the idea that there is competition between Cl^- and —OOC-R. In Fig. 6, the plateau is only observed for C6-Na-10Ca system. At this condition, little adsorption of Cl^- occurs as revealed by the AFM image [20]. Thus, only carboxylate adsorbs to the surface, approaching saturated adsorption at high C6 concentration.

If we consider the magnitudes of the adsorbed amount, assuming that they only come from hexanoate (with a molar weight of 115 g/mole), molecular adsorption densities of 5.5 nm^{-2}, 11.8 nm^{-2}

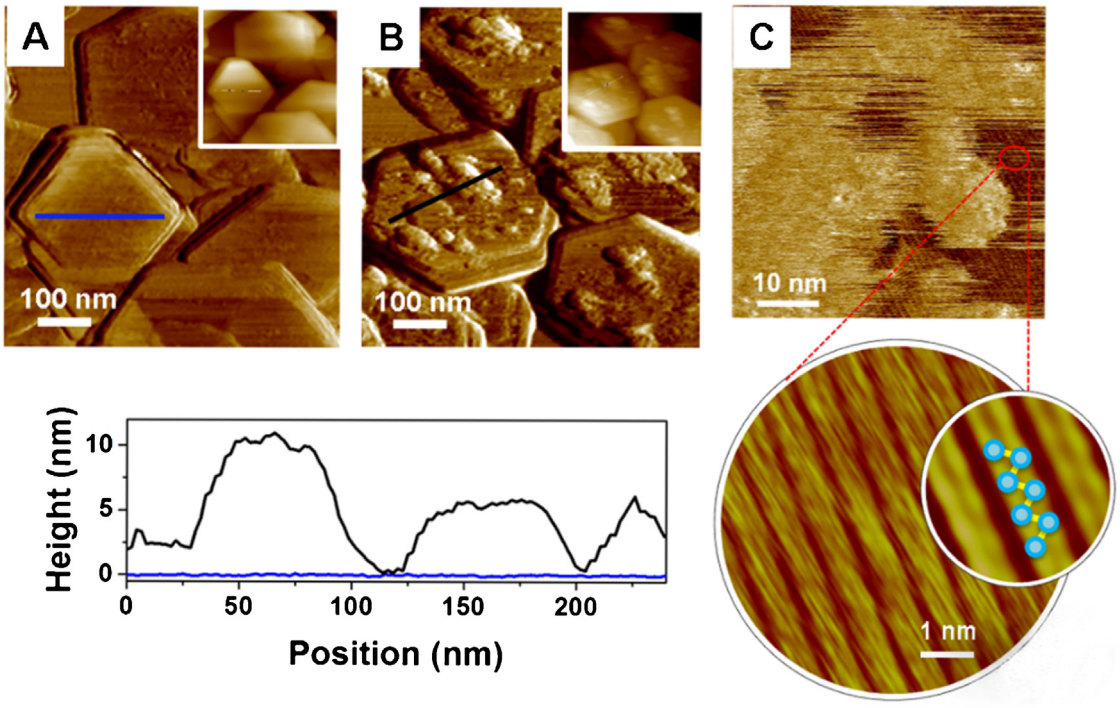

Fig. 7. (A) AFM images of gibbsite particles deposited on silica. (B) In-situ image of hexanoate coated gibbsite particles from 10 mM C6 + 10 mM $CaCl_2$. The line scans compare the local height variations on the platelets, before and after adsorption of C6. (C) presents zoom-ins of the adsorbed hexanoate layer and the adsorbed calcium ions.

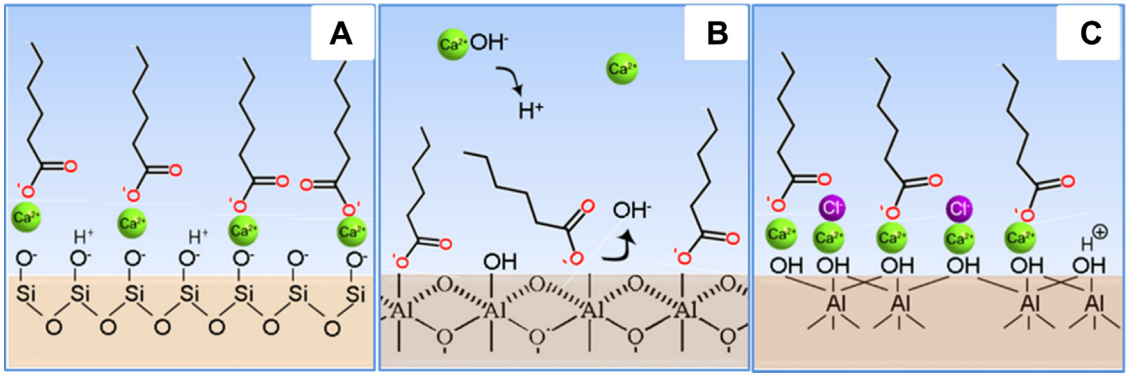

Fig. 8. Schematic illustration of hexanoate adsorption mechanisms at solid-liquid interfaces: (A) silica; (B) alumina; (C) gibbsite. Calcium ions: green symbols; and chloride ions: purple symbols. (For interpretation of the references to color in this figure legend, the reader is referred to the web version of this article.)

and 5.6 nm^{-2} are found for the C6-Na, C6-Na-10Ca and C6-Na-20Ca solutions. The size of a carboxylate head group is around 20 $Å^2$ [19], which corresponds to 5 nm^{-2}. This indicates that with C6-Na-10Ca solutions, adsorbed masses larger than the amount corresponding to a dense monolayer, are achieved. Moreover, the AFM images in Fig. 7 show that the height of the adsorbed layer exceeds the molecular length of the hexanoate. These observations suggest that adsorption takes place in the form of a multilayer. In principle, also water uptake by gibbsite [39] or from the hydrated ions might also contribute to the total adsorbed amount measured. The suggestion of trapped water has been made in several studies [40,41].

In Fig. 8, we summarize the proposed adsorption mechanisms on the three different surfaces. On silica (A), the adsorption of C6 is mainly due to cation bridging, causing the adsorbed amount to increase with the divalent ion concentration, see Fig. 8A. On alumina (B), the adsorption results mainly from ligand exchange, and pH is the dominant factor in this process. Ca^{2+} has a positive influence on the adsorption process, most of which appears to be via the pH: Ca^{2+} ions have the ability to bind with hydroxyl ions in solution acting as buffer ions adjusting the pH. Additionally, some protons at alumina surfaces can be replaced by Ca^{2+}. Since Ca^{2+} also adsorbs onto the alumina surface, we cannot completely rule out (modest) contributions by ion bridging. The adsorption of C6 on gibbsite (C) in presence of (mixed) salts shows a more complex phenomenology. Ca^{2+} ions adsorb to gibbsite, thereby creating adsorption sites for C6. Anions (Cl^- and Hexanoate) compete for these adsorption sites, resulting in a non-monotonous dependence on $CaCl_2$ concentration.

Overall, from our observations in this work, it is clear that divalent cations such as Ca^{2+} are important for carboxylate adsorption, either acting as bridging ions, or as buffering ions adjusting the pH. This corresponds well to the observations in low salinity water flooding process, where low concentrations of divalent ions is a key element [6,42]. As pointed out in this work, the adsorbed layer contains not only carboxylate, but also some ions like Cl^-, or Ca^{2+}. To further investigate the composition of the adsorbed layer, other techniques like ellipsometry, SPR, or XPS etc. could be exploited, to confirm the adsorption mechanisms we proposed here.

4. Conclusions

Quartz Crystal Microbalance (QCM) was exploited to study the adsorption of Hexanoate on different substrates: silica, alumina and gibbsite. Specific focus of this paper was on the effects of Ca^{2+} ions (besides omnipresent Na^+ ions) on the mechanism of carboxylate adsorption. We found that the adsorption is not simply driven by electrostatic interactions. On the negatively charged silica, bridging by Ca^{2+} ions plays a very important role; while on positively charged alumina, adsorption of carboxylate takes place via a ligand exchange process, mainly controlled by the solution pH. Ion bridging might also occur, but it does not play a significant role. Compared to a bare silica surface, the presence of gibbsite can significantly enhance the adsorption. In this case, Ca^{2+} ions first adsorb to the surface forming a double row structure; anions (Cl^- and hexanoate) in the solution then bind to this pre-adsorbed calcium, competing for the adsorption sites. This results in a non-monotonic dependence of hexanoate adsorption on $CaCl_2$ concentration. The oxides studied in this work, silica, alumina and gibbsite can be seen as clay model surfaces, and the carboxylates are important polar components in oil reservoirs. So the understanding of the adsorption process with these simple model systems in electrolytes will shed some light on real rock reservoir, helping to understand the low salinity effects during water flooding in enhanced oil recovery.

Acknowledgements

We thank Dr. Dirk van den Ende for helpful discussion of the QCM data analysis. Financial support was provided through the Exploratory Research (ExploRe) program of BP plc.

References

[1] F. Mugele, B. Bera, A. Cavalli, I. Siretanu, A. Maestro, M. Duits, M.A. Cohen Stuart, D. van den Ende, I. Stocker, I. Collins, Ion adsorption-induced wetting transition in oil–water–mineral systems, Sci. Rep. (2015) 5.
[2] P.F. Luckham, S. Rossi, The colloidal and rheological properties of bentonite suspensions, Adv. Colloid Interface Sci. 82 (1–3) (1999) 43–92.
[3] S.A. Boyd, M.M. Mortland, C.T. Chiou, Sorption characteristics of organic compounds on hexadecyltrimethylammonium-smectite, Soil Sci. Soc. Am. J. 52 (3) (1988) 652–657.
[4] B. Kasprzyk-Hordern, Chemistry of alumina, reactions in aqueous solution and its application in water treatment, Adv. Colloid Interface Sci. 110 (1–2) (2004) 19–48.
[5] E. Manias, A. Touny, L. Wu, K. Strawhecker, B. Lu, T.C. Chung, Polypropylene/montmorillonite nanocomposites: review of the synthetic routes and materials properties, Chem. Mater. 13 (10) (2001) 3516–3523.
[6] A. Lager, K.J. Webb, I.R. Collins, D.M. Richmond, LoSal enhanced oil recovery: evidence of enhanced oil recovery at the reservoir scale, Soc. Pet. Eng. (2016).
[7] L. Wang, S. Liu, T. Wang, D. Sun, Effect of poly(oxypropylene) diamine adsorption on hydration and dispersion of montmorillonite particles in aqueous solution, Colloids Surf. A Physicochem. Eng. Aspects 381 (1–3) (2011) 41–47.
[8] K.N. Han, T.W. Healy, D.W. Fuerstenau, The mechanism of adsorption of fatty acids and other surfactants at the oxide-water interface, J. Colloid Interface Sci. 44 (3) (1973) 407–414.
[9] R. Kummert, W. Stumm, The surface complexation of organic acids on hydrous γ-Al_2O_3, J. Colloid Interface Sci. 75 (2) (1980) 373–385.
[10] H.-L. Yao, H.-H. Yeh, Fumarate, maleate, and succinate adsorption on hydrous δ-Al_2O_3. 2. Electrophoresis observations and ionic-strength effects on adsorption, Langmuir 12 (12) (1996) 2989–2994.
[11] H.-L. Yao, H.-H. Yeh, Fumarate, Maleate, and succinate adsorption on hydrous δ-Al_2O_3. 1. Comparison of the adsorption maxima and their significance, Langmuir 12 (12) (1996) 2981–2988.

[12] J. van den Brand, O. Blajiev, P.C.J. Beentjes, H. Terryn, J.H.W. de Wit, Interaction of anhydride and carboxylic acid compounds with aluminum oxide surfaces studied using infrared reflection absorption spectroscopy, Langmuir 20 (15) (2004) 6308–6317.
[13] A.A. Zaman, R. Tsuchiya, B.M. Moudgil, Adsorption of a low-molecular-weight polyacrylic acid on silica, alumina, and kaolin, J. Colloid Interface Sci. 256 (1) (2002) 73–78.
[14] J. Rosenqvist, K. Axe, S. Sjöberg, P. Persson, Adsorption of dicarboxylates on nano-sized gibbsite particles: effects of ligand structure on bonding mechanisms, Colloids Surf. A Physicochem. Eng. Aspects 220 (1–3) (2003) 91–104.
[15] A. Malgat, J.-P. Boisvert, C. Daneault, Specific influence of univalent cations on the ionization of alumina-coated TiO_2 particles and on the adsorption of poly(acrylic) acid, J. Colloid Interface Sci. 269 (2) (2004) 320–328.
[16] K.M.S. Juhl, N. Bovet, T. Hassenkam, K. Dideriksen, C.S. Pedersen, C.M. Jensen, D.V. Okhrimenko, S.L.S. Stipp, Change in organic molecule adhesion on α-Alumina (Sapphire) with change in NaCl and $CaCl_2$ solution salinity, Langmuir 30 (29) (2014) 8741–8750.
[17] G.-Q. Tang, N.R. Morrow, Influence of brine composition and fines migration on crude oil/brine/rock interactions and oil recovery, J. Pet. Sci. Eng. 24 (2–4) (1999) 99–111.
[18] P.C. Myint, A. Firoozabadi, Thin liquid films in improved oil recovery from low-salinity brine, Curr. Opin. Colloid Interface Sci. 20 (2) (2015) 105–114.
[19] N. Kumar, L. Wang, I. Siretanu, M. Duits, F. Mugele, Salt dependent stability of stearic acid Langmuir–Blodgett films exposed to aqueous electrolytes, Langmuir 29 (17) (2013) 5150–5159.
[20] I. Siretanu, D. Ebeling, M.P. Andersson, S.S. Stipp, A. Philipse, M.C. Stuart, D. Van Den Ende, F. Mugele, Direct observation of ionic structure at solid–liquid interfaces: a deep look into the stern layer, Sci. Rep. (2014) 4.
[21] A.M. Wierenga, Aqueous dispersions of colloidal gibbsite platelets: synthesis, characterisation and intrinsic viscosity measurements, Colloids Surf. A Physicochem. Eng. Aspects 134 (3) (1998) 359–371.
[22] F. Liu, C. Zhao, F. Mugele, D. Van Den Ende, Amplitude modulation atomic force microscopy, is acoustic driving in liquid quantitatively reliable? Nanotechnology 26 (38) (2015) 385703.
[23] C. Zhao, D. Ebeling, I. Siretanu, D. van den Ende, F. Mugele, Extracting local surface charges and charge regulation behavior from atomic force microscopy measurements at heterogeneous solid-electrolyte interfaces, Nanoscale (2015).
[24] J.S. Lumsden, XXXIV—solubilities of the calcium salts of the acids of the acetic series, J. Chem. Soc. Trans. 81 (1902) 350–362.
[25] H. Stephen, T. Stephen, Solubilities of Inorganic and Organic Compounds, vol. 1, Pergamon Press, Oxford, 1963.
[26] S.Y. Lee, R. Welbourn, S.M. Clarke, M.W.A. Skoda, L. Clifton, A. Zarbakhsh, Adsorption of sodium hexanoate on α-alumina, J. Colloid Interface Sci. 407 (0) (2013) 348–353.
[27] S.M. Bulatovic, Handbook of Flotation Reagents: Chemistry, Theory and Practice vol. 1: flotation of sulfide ores, Elsevier, 2007.
[28] P. Mukerjee, K.J. Mysels, Critical Micelle Concentrations of Aqueous Surfactant Systems, DTIC Document, 1971.
[29] G. Sauerbrey. The Use of Quartz Crystal Oscillators for Weighing Thin Layers and for Microweighing Applications (1959).
[30] M. Rodahl, F. Höök, C. Fredriksson, C.A. Keller, A. Krozer, P. Brzezinski, M. Voinova, B. Kasemo, Simultaneous frequency and dissipation factor QCM measurements of biomolecular adsorption and cell adhesion, Faraday Discuss. 107 (1997) 229–246.
[31] M.V. Voinova, M. Rodahl, M. Jonson, B. Kasemo, Viscoelastic acoustic response of layered polymer films at fluid-solid interfaces: continuum mechanics approach, Phys. Scr. 59 (5) (1999) 391.
[32] A.K. Bickerstaffe, N.P. Cheah, S.M. Clarke, J.E. Parker, A. Perdigon, L. Messe, A. Inaba, The crystalline structures of carboxylic acid monolayers adsorbed on graphite, J. Phys. Chem. B 110 (11) (2006) 5570–5575.
[33] B. Borovsky, B.L. Mason, J. Krim, Scanning tunneling microscope measurements of the amplitude of vibration of a quartz crystal oscillator, J. Appl. Phys. 88 (7) (2000) 4017–4021.
[34] C.W. Davies, 56. The extent of dissociation of salts in water. Part VI. Some calcium salts of organic acids, J. Chem. Soc. (Resumed) (0) (1938) 277–281.
[35] D.R. Lide, CRC Handbook of Chemistry and Physics, CRC Press, 2004.
[36] X. Wang, S.Y. Lee, K. Miller, R. Welbourn, I. Stocker, S. Clarke, M. Casford, P. Gutfreund, M.W.A. Skoda, Cation bridging studied by specular neutron reflection, Langmuir 29 (18) (2013) 5520–5527.
[37] B.K.G. Theng, Formation and Properties of Clay-polymer Complexes, vol. 4, Elsevier, 2012.
[38] K. Vermöhlen, H. Lewandowski, H.D. Narres, E. Koglin, Adsorption of polyacrylic acid on aluminium oxide: DRIFT spectroscopy and ab initio calculations, Colloids Surf. A Physicochem. Eng. Aspects 170 (2–3) (2000) 181–189.
[39] F. Adekola, M. Fédoroff, H. Geckeis, T. Kupcik, G. Lefèvre, J. Lützenkirchen, M. Plaschke, T. Preocanin, T. Rabung, D. Schild, Characterization of acid-base properties of two gibbsite samples in the context of literature results, J. Colloid Interface Sci. 354 (1) (2011) 306–317.
[40] L. Macakova, E. Blomberg, P.M. Claesson, Effect of adsorbed layer surface roughness on the QCM-D response: focus on trapped water, Langmuir 23 (24) (2007) 12436–12444.
[41] X. Liu, D. Wu, S. Turgman-Cohen, J. Genzer, T.W. Theyson, O.J. Rojas, Adsorption of a nonionic symmetric triblock copolymer on surfaces with different hydrophobicity, Langmuir 26 (12) (2010) 9565–9574.
[42] K.S. Sorbie, I. Collins, A Proposed Pore-Scale Mechanism for How Low Salinity Waterflooding Works, Society of Petroleum Engineers, 2016.